



Improving Hydrocarbon Prospect Evaluation at Badr El Din-3 and Badr El Din-15 Oil Fields by Integrating 3D Structural Modeling and Petrophysical Analysis for Abu-Gharadig Basin, North of Western Desert, Egypt

Mohamed A. Taha¹ · Tharwat H. Abdelhafeez² · Sherif M. El-hady¹ · Ahmed Z. Nooh³ · Waheed H. Mohamed²

Received: 12 April 2022 / Accepted: 5 June 2022 / Published online: 19 July 2022
© The Author(s) 2022

Abstract

The BED-3 and BED-15 oil fields are situated in the northwestern portion of the Abu-Gharadig sedimentary basin. The Basin is an E–W trending intracratonic rift basin and ranges in age between the Late Jurassic and Early Cretaceous. Significant extension events, followed by subsidence, took place throughout the Middle Jurassic and continued to the Cretaceous. The relative movement of Africa toward Laurasia in the Jurassic changed from eastward to westward between the Early Cretaceous and the Santonian. Therefore, a compressive force due to the change in direction affected the African plate and gave rise to the reversal of basins (such as the Abu-Gharadig sedimentary basin). Inverted anticlines are important structural traps for hydrocarbons that were formed by the compressional forces acting on the Abu-Gharadig sedimentary basin. This study primarily focuses on understanding the BED-3 and BED-15 fields' structural style, in addition to the subsurface structure that has participated in the petroleum accumulation in the Abu-Roash C Member (Abu-Roash Formation) in the oil fields, in order to maximize oil recovery in these two fields through new wells. The aim of this study was achieved based on information from 30 two-dimensional seismic profiles integrated with well log data from nine boreholes. The Abu-Roash C reservoir represented by two horizons, in addition to minor and major faults, are recognized and marked. Structural trend in the study area ranges from ESE–WNW to NW–SE, and structures consist of folds and faults, forming horsts, grabens, and half-grabens, all of which are favorable for hydrocarbon accumulation. The petrophysical analysis performed on the BED3-8 well shows approximately 87.4% hydrocarbon saturation within the reservoir rock, while the hydrocarbon saturation of the available wells in BED-15 is calculated to vary between 56.1 and 78.8%. Hence, this study suggests that BED-3 and BED-15 oilfields have an excellent chance of producing hydrocarbons.

Keywords Petrophysical analysis · Abu-Gharadig basin · Fault interpretation · Inverted anticline · Structure model · Seismic interpretation

1 Introduction

Hydrocarbons (natural gas and oil) are the most important conventional energy sources in the world and constitute significant incomes for the producing countries. Therefore, all countries are interested in the exploration of hydrocarbons. However, the oil well drilling process is a very expensive operation. Then, a careful assessment of the petroleum system is necessary for a successful exploration by drilling in the target area. Seismic reflection integrated with well-logging data is the most appropriate method to achieve this target. The Abu-Gharadig sedimentary basin is the largest basin with important petroleum potential in the northern part of

✉ Mohamed A. Taha
mohamed.taha@nriag.sci.eg, mohamedtaha2070@yahoo.com

¹ Department of Seismology, National Research Institute of Astronomy and Geophysics (NRIAG), Helwan, Cairo 11421, Egypt

² Geology Department, Faculty of Sciences, Al Azhar University, Cairo, Egypt

³ Egyptian Petroleum Research Institute (EPRI), Nasr City, Cairo, Egypt



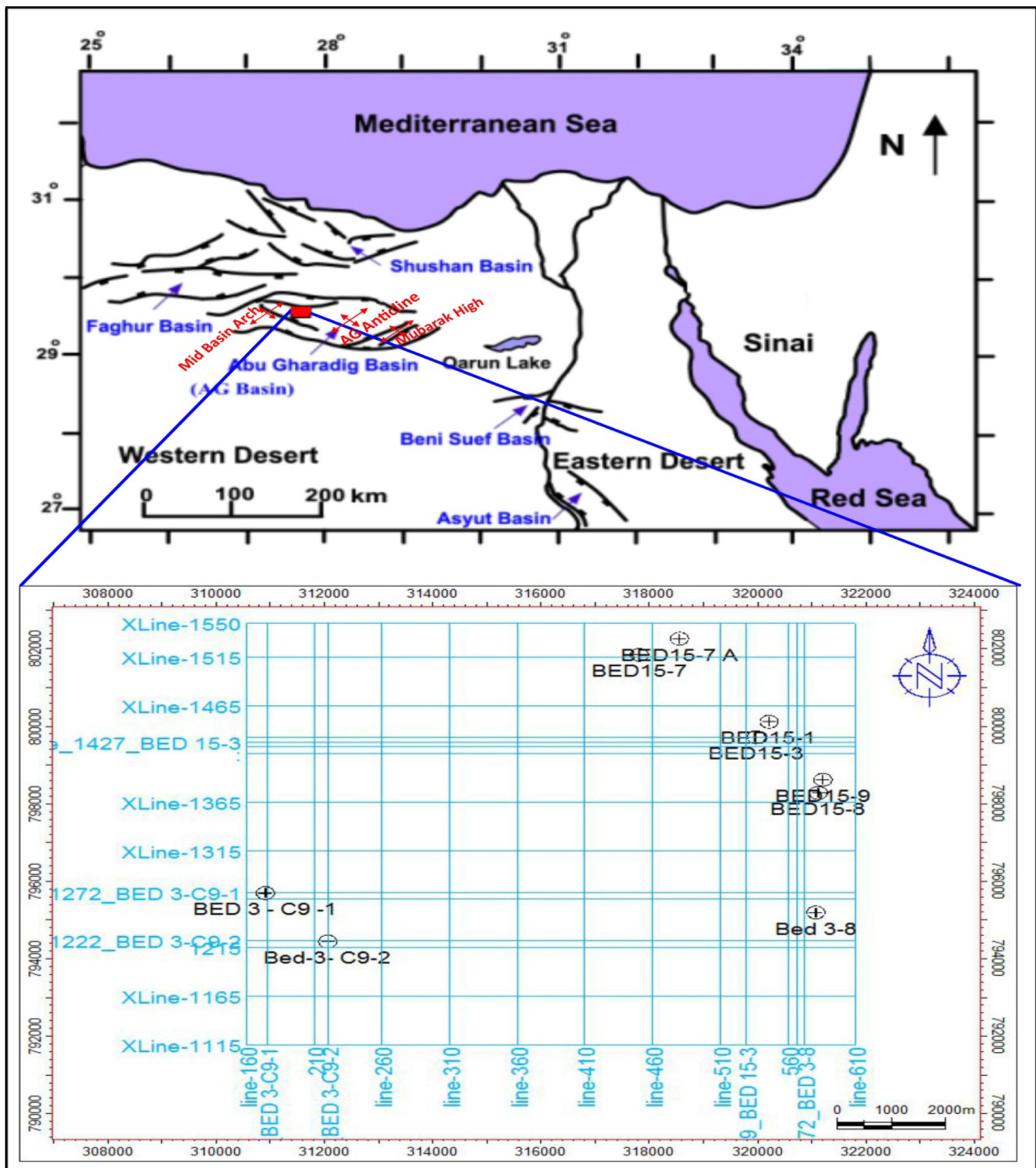


Fig. 1 Location of the study area, along with a base map displaying the locations of the available wells and seismic sections

the Egyptian Western Desert [1]. The study area is located in the northwestern portion of the Abu-Gharadig sedimentary basin, between latitudes $29^{\circ} 47' N$ and $29^{\circ} 54' N$ and longitudes $27^{\circ} 50' E$ and $27^{\circ} 58' E$ (Fig. 1). The Abu-Gharadig sedimentary basin is E–W-oriented with an area of approximately 60 km by 300 km, covering 3.6% of the Egyptian

Western Desert. The age of the basin ranges from the Late Jurassic to the Early Cretaceous Period [2]. The core of the Abu-Gharadig sedimentary basin expands between the Kattaniya horst toward the east and the Qattara Depression toward the west; it evolved as an intra-cratonic half-graben system that is elongated asymmetrically and E–W trending

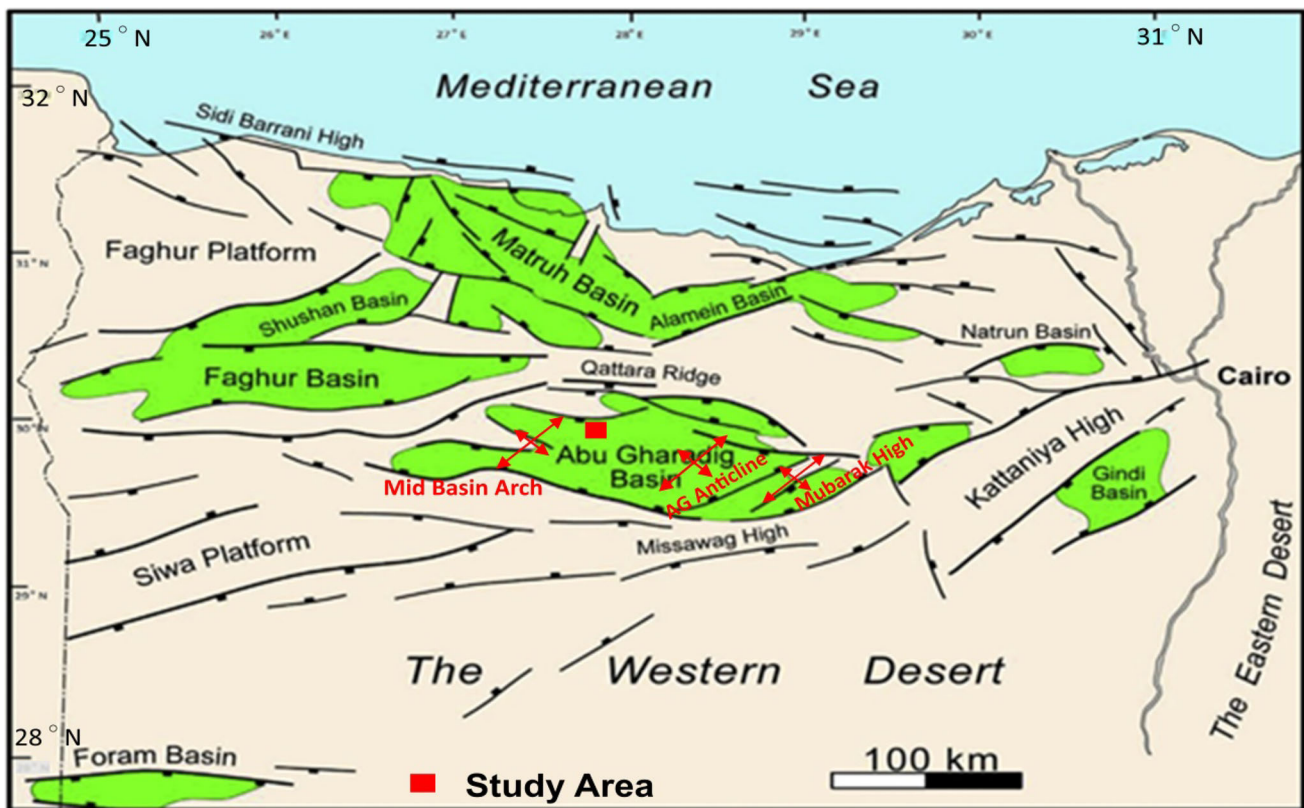


Fig. 2 Location of the Mesozoic and Early Cenozoic basins (green areas) and structural trends in the northern part of the Western Desert of Egypt [24]; Universal Transverse Mercator Zone 35 projection

and bounded by the Sitra Platform toward the south and Qattara Ridge toward the north (Fig. 2). A sinistral wrenching prevailed during the Early Cretaceous produced a NE–SW group of normal faults [3]. This was followed throughout the Late Cretaceous by a reversal tectonic event [4–7]. Dextral wrenching during the inversion stress occurred in the area and the associated wrenching produced NE–SW oriented compressive structures, such as the Abu-Gharadig anticline and the Mid Basin Arch as well as by extensional structures oriented WNW to ESE and NW to SE [8]. Because of these tectonic movements, a normal fault group trending NW and WNW dissected the basin. They split the area into isolated fault blocks, such as the BED-15 and BED-17 structures oriented NE [8]. The primary focus of this study is to understand the structural style of the BED-3 and BED-15 fields, in addition to the subsurface structure, which has participated in the petroleum accumulation at the Turonian Abu-Roash C Member (Abu-Roash Formation) in the BED-3 and BED-15 oil fields. This study aims to integrate available wire-line log data with seismic reflection data for estimating the petroleum potential of the study area.

2 Geological Setting

Many research studies have been performed on the Abu-Gharadig sedimentary basin which has explained the basin's geological and tectonic setting (e.g., [1, 4, 6, 7, 9–11]).

2.1 Structural Features

The sedimentary basins included in the northern part of the Western Desert comprise two districts in the south and north, separated by the E–W to ENE trending uplift of Ras Qattara–North Sinai [3]. The prevailing structural characteristics of the Abu-Gharadig sedimentary basin include NE to SW trends that divided the basin into structural features, known as the Mubarak High, the Abu-Gharadig anticline, and the Mid Basin Arch from E to W [12]. Onset of the Abu-Gharadig sedimentary basin formation began during the Late Jurassic with the intrusion of a dolerite mantle bulge and deep-seated basaltic rock; which was related to the early stage of the Alpine Orogeny [1, 2], and continued by extension during the Cretaceous [2, 13–18]. According to Smith (1971), the relative movement of Africa toward Laurasia was eastward in the Jurassic, but subsequently, changed to westward between the Early Cretaceous and the Santonian [2, 19, 20]. As a

result, a compressive event affected the African plate and led to the reversal of basins including the Abu-Gharadig Sedimentary Basin. Inverted anticlines are the evidence of the compressive event that affected the Abu-Gharadig sedimentary basin with a NE–SW trend, and formed the important petroleum traps in the basin. The faults that dissected the basin have E–W, NE–SW, and WNW to ESE trends [21, 22]. There are three types of faults delineated via seismic survey in the basin: strike–slip (right and left lateral), reverse, and normal faults. Normal faults are the most prevalent; the Abu-Gharadig basin is affected by 771 normal faults that trend E–W, W–NW, and E–NE. The reverse faults are relatively few, trending E–W and E–NE. The strike–slip faults are the least common. Often the sense of lateral slip along faults can be determined by matching the structures on both sides of the fault [19, 23]. The maximum displacement on the primary normal faults in the basin reaches 2450 m [19]. Small numbers of folds are also recognized in the basin [8].

2.2 Stratigraphic Framework

The subsurface succession in the northern part of the Western Desert is complete from the Precambrian to the recent as shown in Fig. 3 [8]. The thickness of the sedimentary rocks overlying the Precambrian rocks reaches > 10,600 m within the basin, while the thickness reaches ~ 3000 m in the northern portion of the basin over the Qattara ridge. Generally, the Late Cretaceous stratigraphic succession of this region has been divided in three formations with the Bahariya Formation at the bottom followed by the Abu-Roash Formation in the middle and either the Apollonia or Khoman Formation at the top, whenever Khoman Formation is missing. The mean thicknesses of the Upper Cretaceous successions in the basin are ~ 2100 m [25, 26]. The Abu-Roash Formation is primarily composed of alternating clastics and carbonates that represent regressive and transgressive phases, respectively. The formation is divided into seven lithostratigraphic members, named from top to bottom as A to G, where B, D, and F refer to fairly clean carbonates and the last unit contains altered contents of detrital material (clastics with limestone). The Abu Roash "C" Member is one of the most important reservoirs in the Abu Roash Formation, Abu Gharadig Basin's BED-3 and BED-15 oilfields. The Abu Roash "C" Member reservoir lacks detailed studies. Therefore, a detailed study of this reservoir is needed. This Member is essentially comprised of siltstone, shale, and sandstone with some streaks of limestone. The limestone was deposited in a restricted shallow marine shelf [27]. This member was formed in the Abu-Gharadig sedimentary basin during the Turonian (Late Cretaceous) in a transgression phase that initiated with the Bahariya Formation in the Cenomanian and ended with the Khoman Formation in the Maastrichtian [2].

3 Data and Methodology

This work is based on the integration of two-dimensional (2D) seismic lines and borehole data within the BED-3 and BED-15 oil fields. The Badr El-Din Petrol Company provided data for this study with the permission of EGPC under the Ministry of Petroleum and Mineral Resources. The available seismic data are 30 2D seismic profiles covering the BED-3 and BED-15 oil fields. These profiles are categorized into two groups; the first group of in-line or depositional dip trends contains 15 lines that extend N–S, and each line reaches 10,875 m in length. The second group of cross-line or depositional strike trends contains 15 lines trending E–W, with each line 11,250 m long. Moreover, there are certain arbitrary seismic profiles linking some of the available wells in the study area (see Fig. 1). In addition, the well-logging data provided in las format for nine exploratory wells have been used to discuss the petrophysical parameters and petroleum potential of the study area. These borehole parameters and potentials are shown in Tables 1 and 2, and a check-shot survey is also provided.

The following procedures were followed in this study:

3.1 Seismic Interpretation

The seismic analysis aims to detect target horizons, horizon depth, the subsurface faults, and the structural style of the Abu-Roash C Member. The following workflow is followed for this purpose.

3.1.1 Seismic Well Tie and Horizon Selection

The velocity correlation method is used in this work. The uniqueness of this method is that the correlation between the borehole and the seismic data depends on the velocity values rather than on seismic amplitudes [28, 29]. This method is effective with at least a single well and check-shot survey data and is better than the synthetic seismogram method in the following ways [28]:

- A synthetic seismogram is a simulation of seismic traces by various parameters, which must be tested to obtain the greatest approximation to real traces. The synthetic seismogram method can require a long time to verify the phase, wavelet, and multiples, for each hole, and then to estimate the optimum solution with a mathematical and visual correlation of the seismic data. Furthermore, even in the presence of good responses, a unique specified solution might be acceptable for a slice of the data, whereas another solution might be the optimum fit for another interval.
- For certain projects, especially those with several boreholes, the use of synthetic seismograms may require

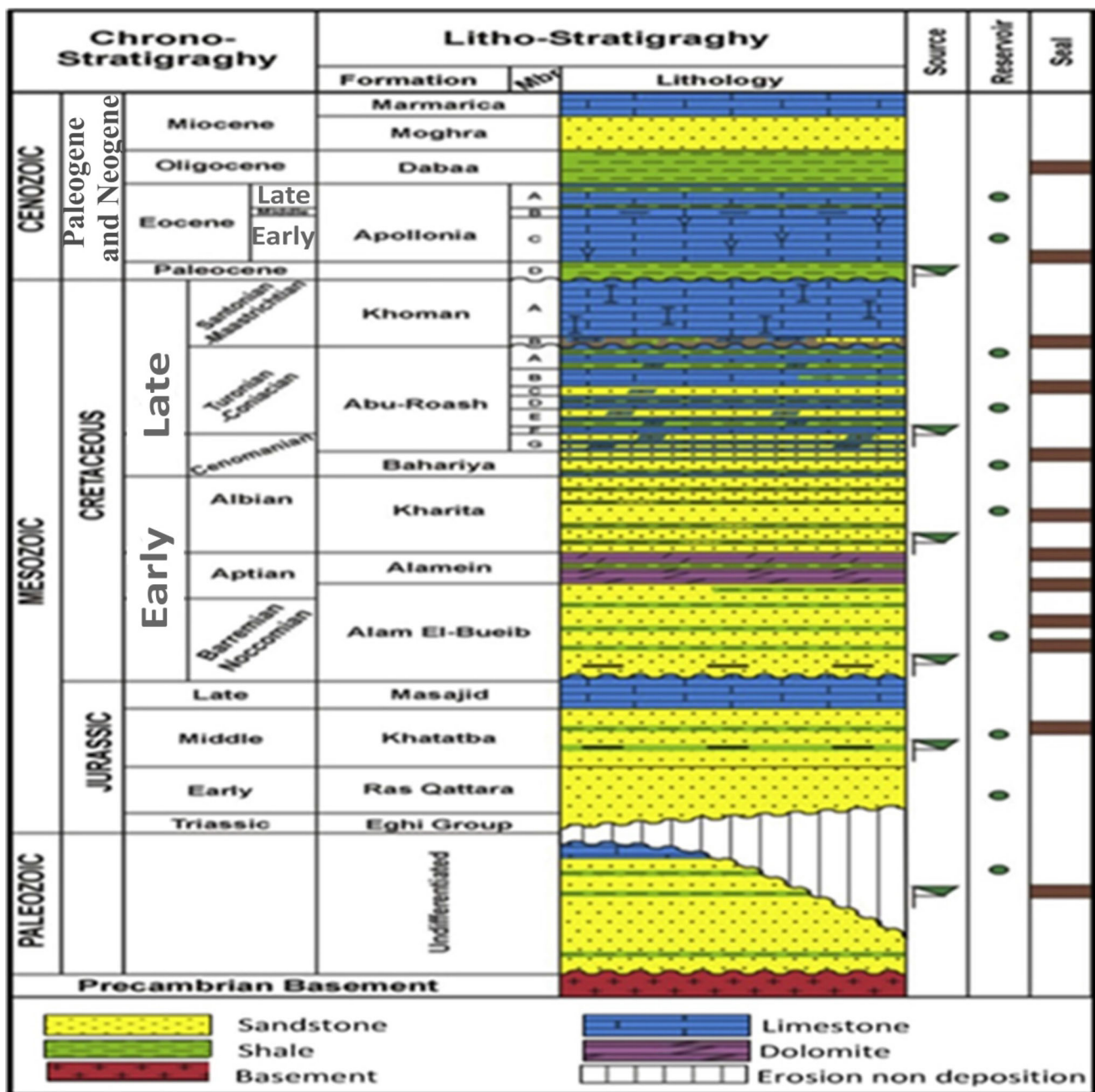


Fig. 3 Generalized lithostratigraphic column of the northern part of the Western Desert of Egypt showing the source, reservoir and seal rocks [18]

individually adjusting each well with the 2D or three-dimensional (3D) seismic data that acts as the reference data. As a result, the borehole data is adjusted as per the seismic line, which creates an unusual environment.

After the seismic-to-well tie process, the formation tops from the drilled wells are matched and plotted on the seismic sections (Figs. 4, and 5). Two horizons (the upper and lower surfaces of Abu-Roash C) are marked and interpreted in the seismic profiles.

3.1.2 Fault Interpretation

The time structures displayed in Fig. 6a and b suggest a general NE–SW trending direction for the anticline. This anticline is dissected by 18 normal faults (although the top of the Abu-Roash C Member is only affected by 16 faults). In general, fault planes trend ESE–WNW to SE–NW. The interpreted normal faults indicate a complex structural style with two primary faults and sixteen minor or secondary faults. The observed area contains a group of parallel nonbranched

Table 1 Reservoir averages per well of BED-3 and BED-15 in the Abu-Roash C Member

Well name	Top (mss)	Base (mss)	Gross reservoir	Net interval	NTG (frac)	Average porosity
BED15-1	3077	3161.92	84.92	24	0.283	20.8
BED15-3	3062	3145.54	83.54	32.04	0.384	18.3
BED15-7	3165.27	3249.44	84.17	22	0.261	23.3
BED15-7A	3504.93	3638.09	133.16	36.59	0.275	23.13
BED15-8	3146	3208.8	62.8	27	0.43	17.8
BED15-9	3125.57	3209.5	83.93	18.93	0.226	20
BED3-8	2981.75	3079.57	97.82	25	0.256	20.03
BED3-C9-A	2997	3054	57	17.26	0.303	18
BED3-C9-2	2996	3067	71	14.3	0.201	16.8

Table 2 Pay averages per well of BED-3 and BED-15 in the Abu-Roash C Member

Well name	Top (mss)	Base (mss)	Net interval	NTG (frac)	V_{sh}	Average porosity	Average S_w	Average S_{hr}
BED15-1	3077	3161.92	5	0.059	6.5	20.7	28.6	71.4
BED15-3	3062	3145.54	21.04	0.252	10	20.15	21.2	78.8
BED15-7	3165.27	3249.44	6	0.071	7	32.6	34	66
BED15-7A	3504.93	3638.09	16.59	0.125	7.3	30.2	32	68
BED15-8	3146	3208.8	6	0.096	7	18	34.3	65.7
BED15-9	3125.57	3209.5	5.93	0.071	10	20.5	43.9	56.1
BED3-8	2981.75	3079.57	11.2	0.1124	8.2	20.8	12.6	87.4
BED3-C9-A	2997	3054	0	0	12	–	–	–
BED3-C9-2	2996	3067	0	0	11	–	–	–

normal faults on the seismic profiles with some minor faults divided into smaller segments. Some of these faults are synthetic faults, with downthrows in equivalent directions such as the main faults, and others are antithetic faults with downthrow in the opposite direction.

3.1.3 Mapping of Selected Traveltimes

Two-way travel time (TWT) surfaces are created for the top and bottom of the Abu-Roash C Member (Fig. 6a and b).

3.1.4 Depth Conversion

The horizon's depth surfaces are obtained from the TWT surfaces using the time–depth relation generated from the check-shot data (Fig. 7). As shown in the depth maps (Fig. 8c and d), the area at the center, which is dissected by the two major faults, and the part of the map that extends from the SW to the center, is shallower. However, the other parts of the study area are deeper with depths from ~ 75 m to > 200 m in the NE and SE sectors (Fig. 6c and d). The two depth surfaces are subtracted to get an isopach surface map of the Abu-Roash C Member (Fig. 8). As per Fig. 8, the study area

can be subdivided into two parts; the thicker BED-3 in the south and the thinner BED-15 in the north.

3.1.5 3D Seismic Modeling

The outputs of the seismic analysis are exploited during the structural modeling procedure as input data. The model building is divided into three primary steps, of which the fault modeling process is the first. The fault modeling process delineates the faults in the model and is the basis for the 3D gridding. Fault modeling involved the generation of important pillars over all the fault planes to merge them into the model. A key pillar is a line with high, middle, and low points. A set of key pillars separately defined each fault. The second step is the pillar gridding. This process creates the structural grids through the fault model. The gridding begins by generating a 2D grid (called a skeleton) among all the middles of the pillars. Then, the upper and base grids are created from the highest and lowest points of the key pillars; this forms connections among all the faults defined in the fault model. The third step is making a horizon that represents the base of the vertical layering in the model. This process creates distinct geological horizons from the entrance data in XYZ. The input data represent surfaces at the depths of

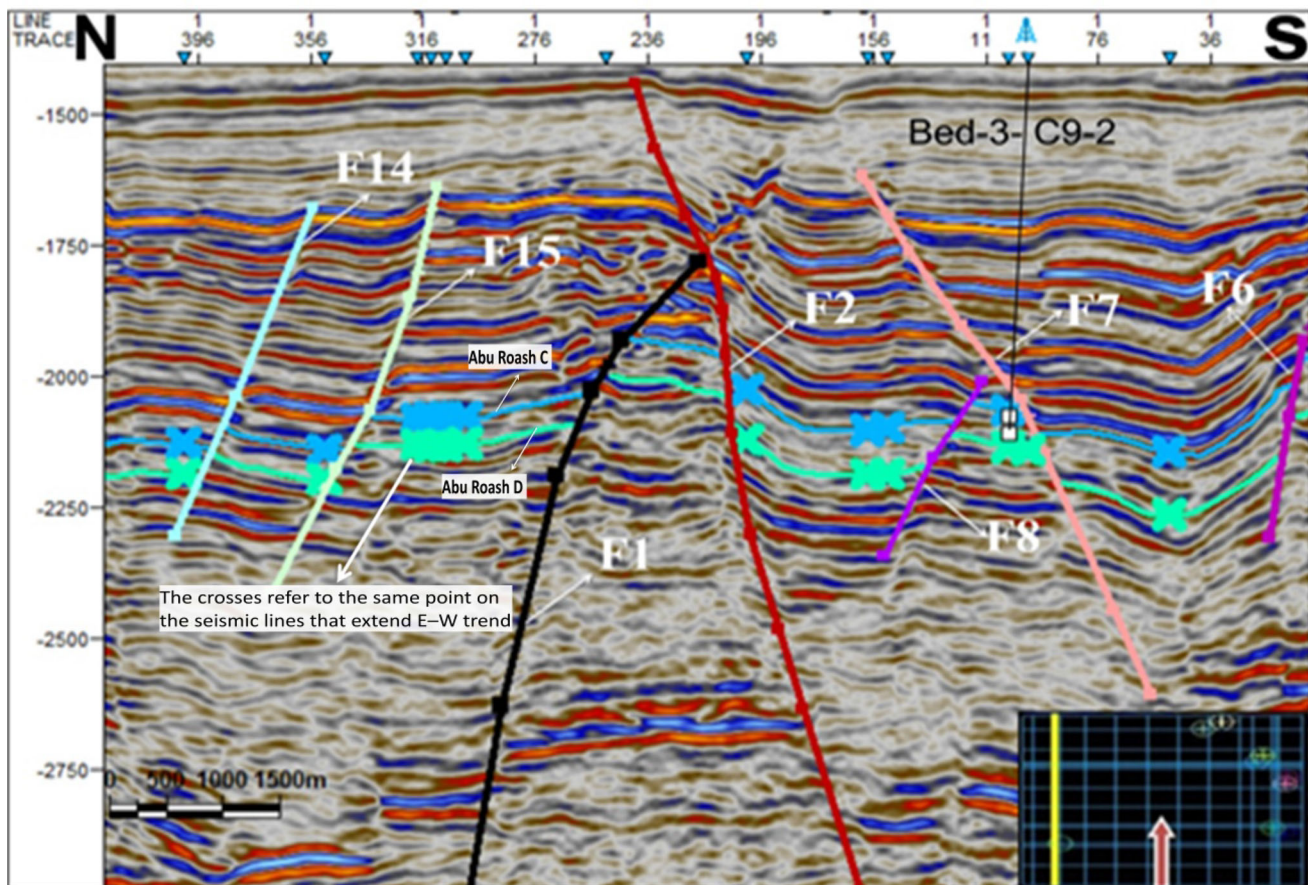


Fig. 4 Interpreted 2D seismic profile (in-line No. 210) passing through BED3-C9-2 well along N–S trend

the top and bottom of the Abu-Roash C Member. The last output is a 3D seismic structural model from the top of the Abu-Roash C Member showing depths, faulting, and other structures in 3D (Fig. 9).

3.2 Petrophysical Analysis

Petrophysical analyses were performed using available logging data (gamma ray, spontaneous potential, density, neutron, and resistivity) for the Abu-Roash C Member in nine wells. The analyses evaluated the shale volume, porosity, and saturation of water and hydrocarbon. All of these parameters are more important in delineating the reservoir petroleum potential. To perform the petrophysical evaluation for wells in BED-3, the following parameters have been employed: $a = 1$, m (cementation exponent) = n (saturation exponent) = 2, $R_w = 0.03$ Ohm-m at 104.4 °C, and 24 °C at the surface. Core samples were acquired over A/R'' C'' formation from the wells BED 15-3, BED 15-7, and BED 3–8 and incorporated into the study. From the special core analysis in BED-15, the values of m and n in BED-15 were obtained, in which $a = 1$, $m = 2$, and $n = 1.85$; $R_w = 0.04$ Ohm-m at wells BED 15-7 and BED 15-7A while $R_w = 0.07$ Ohm-m at wells BED 15-1 and

BED 15-3. The reservoir temperature was measured during the initial production test of well BED 15-1 to be 107.8 °C at 3137 mss. The static surveys, which were performed in the new wells, demonstrated that the reservoir temperature is 111.1 °C.

3.2.1 Volume of Shale (V_{sh})

In this study, a gamma-ray log was used to determine the volume of shale using Eq. (1). The available well logging data of the Abu-Roash C Member show high-level gamma-ray and neutron porosity log responses as detected against the zones of high shale content.

$$V_{shGR} = \frac{GR_{max} - GR_{log}}{GR_{max} - GR_{min}} \quad (1)$$

3.2.2 Porosity and Water Saturation (S_w)

The porosity is calculated by weighted average neutron density using a shale correction. The water saturation was

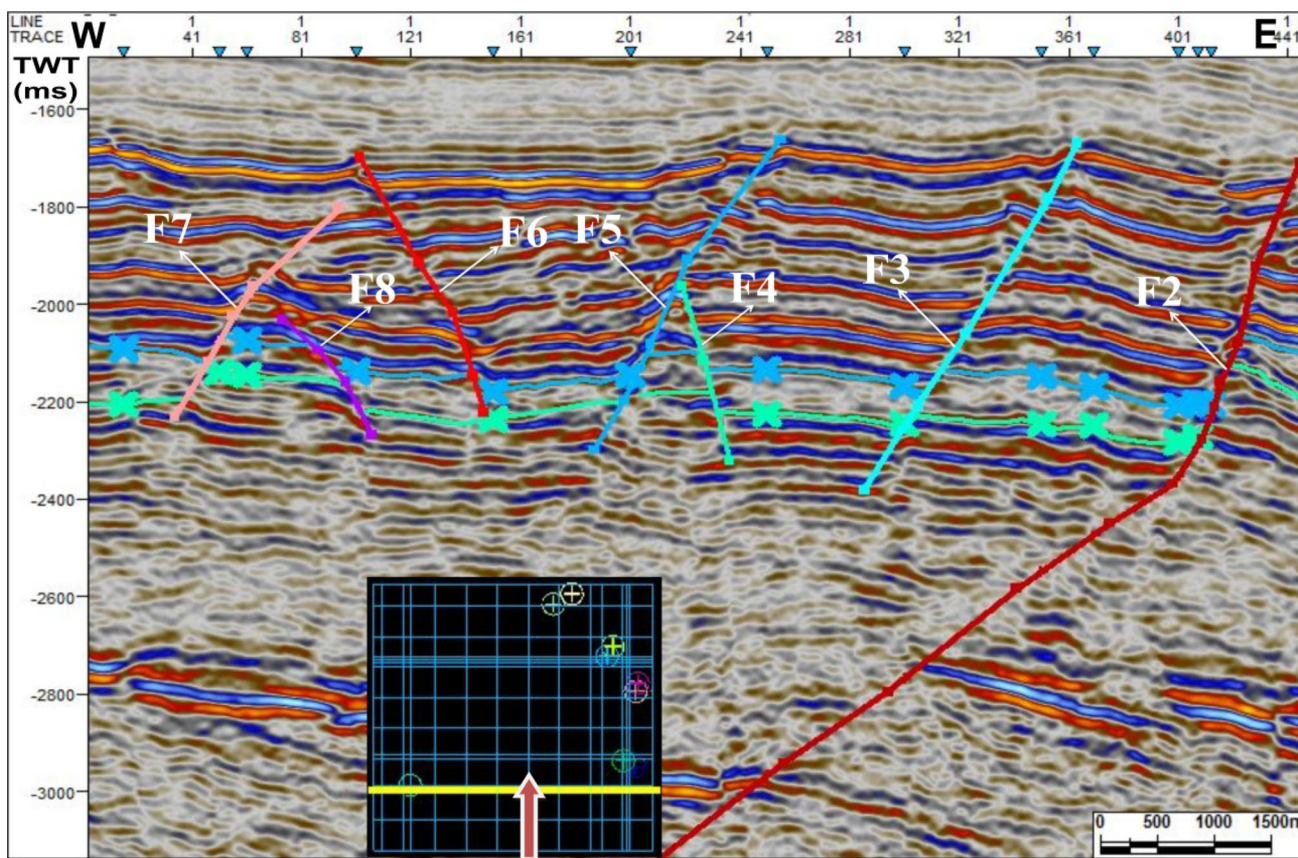


Fig. 5 Interpreted 2D seismic profile (cross-line No. 1215) along E–W trend

calculated via Archie’s equation Eq. (2):

$$S_w^n = \frac{R_w}{(\phi^m \times R_f)} \tag{2}$$

3.2.3 Hydrocarbon Saturation (S_{hr})

The petroleum saturation is calculated at a specified temperature by Eq. (3):

$$\text{Hydrocarbon Saturation} = S_{hr} = 1 - S_w \tag{3}$$

4 Results and Discussion

4.1 Seismic Evaluation Model

In structural geology, basin inversion is associated with the relative uplift of a sedimentary basin or associated structure because of crustal shortening. Generally, uplift in the footwalls of earlier extensional faults or uplift caused by mantle plumes is excluded. Inversion may show distinct faults in

which the original movement of an extensional fault became reactivated in the reverse direction. Occasionally, the term negative inversion can be used to define the reactivation of thrust faults and reversals through extension. Finally, in some cases, the word inversion simply shows that a relatively low-lying region is uplifted while the stratigraphic sequence itself is not usually inverted. Fault polygons and depth surfaces are used to develop a 3D seismic structural model of the top of the Abu-Roash C Member, illustrating the faulting, depths, and other structures in 3D as a product of this study. Moreover, multiple cross-sections are created in various orientations (Fig. 10a–d) to define the structural situation of the Abu-Roash C Member in the study area. The results indicate that study area is intersected by two major normal faults and sixteen minor normal faults that formed horsts, grabens, and half-grabens, which are promising hydrocarbon accumulation sites. In general, NE–SW trend prevailed in the structural characteristics of the basin and divided the basin into the structural elements called from E to W the Mubarak High, Abu-Gharadig anticline, and the Mid Basin Arch. Inverted anticlines trending NE–SW represent the compression force that acted on the Abu-Gharadig sedimentary basin; the inverted anticlines exemplify the important petroleum traps within the basin. At the top of the Abu-Roash

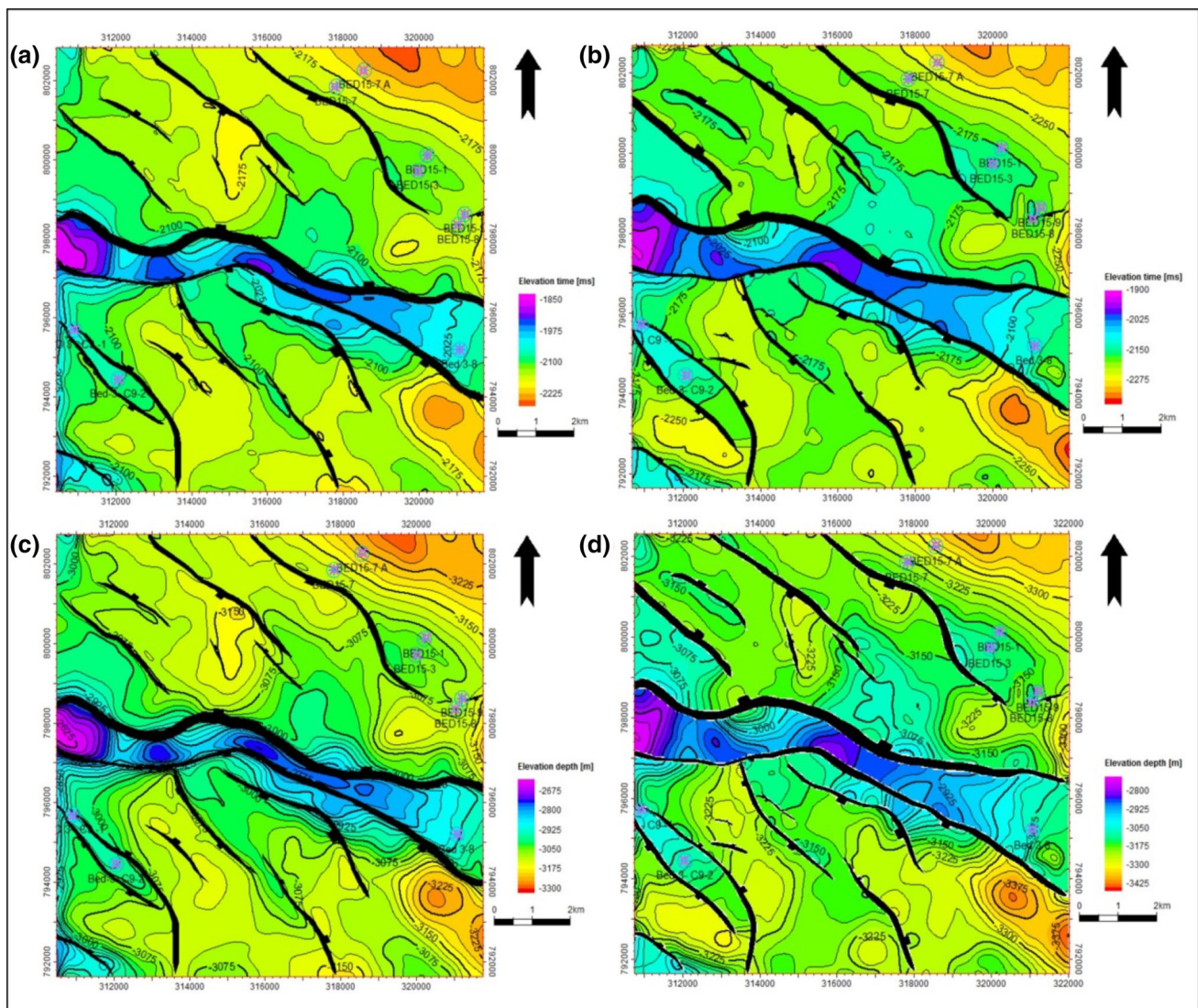


Fig. 6 a and c the time and depth maps for the top of Abu-Roash C unit and b, d the time and depth maps for the bottom of the Abu-Roash C Member

C Member, the travel time structure maps suggest a general anticline-trending NE–SW, indicating that the area has been affected by NW–SE compression. In general, the fault planes have trends ranging from ESE–WNW to NW–SE. A number of growth faults are identified in this study that indicate the action of syndimentary tectonics. The dominant structural elements affecting the top of the Abu-Roash C Member are outlined in (Fig. 11a and b).

4.2 Petrophysics and Hydrocarbon Potential Evaluation

4.2.1 Petrophysical Properties of Reservoir Rocks

Tables 1 and 2 summarize the reservoir and pay averages per well of Abu-Roash C Member in the BED-3 and BED-15

fields. Table 2 outlines the average petrophysical parameters of the Abu-Roash C Member in selected wells in the BED-3 and BED-15 fields. As per the estimations of the petrophysical properties for the selected wells, the shale content or volume (V_{sh}) analysis of the Abu-Roash C Member sandstone in the BED-15 wells illustrates the relatively slight shale content with an average of 7%, a minimum of 6.5%, and a maximum of 10%. The Abu-Roash C Member sandstone in the BED-3 wells shows an average shale content of 10%, a minimum of 8.2%, and a maximum of 12%. However, the effective porosity (ϕ_{eff}) interpretation of the Abu-Roash C Member sandstone presents a moderate value of 23% with a maximum of 32.6% in the BED 15-7 well. Abu-Roash C Member sandstone demonstrates good porosity in BED 3-8 well, averaging 20.8%. The water saturation (S_w) averages

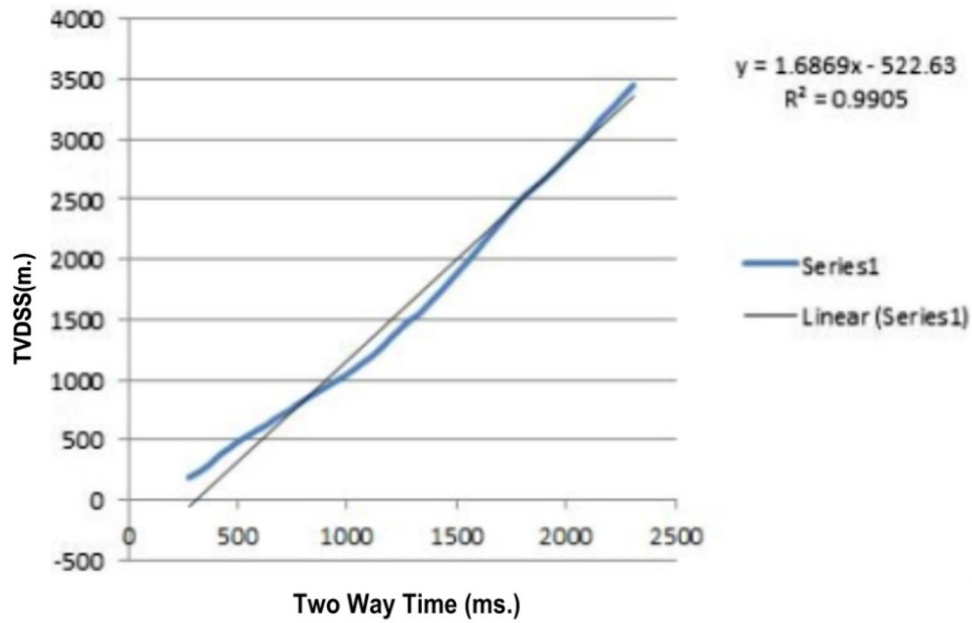


Fig. 7 Time–depth chart, generated from the check-shot survey

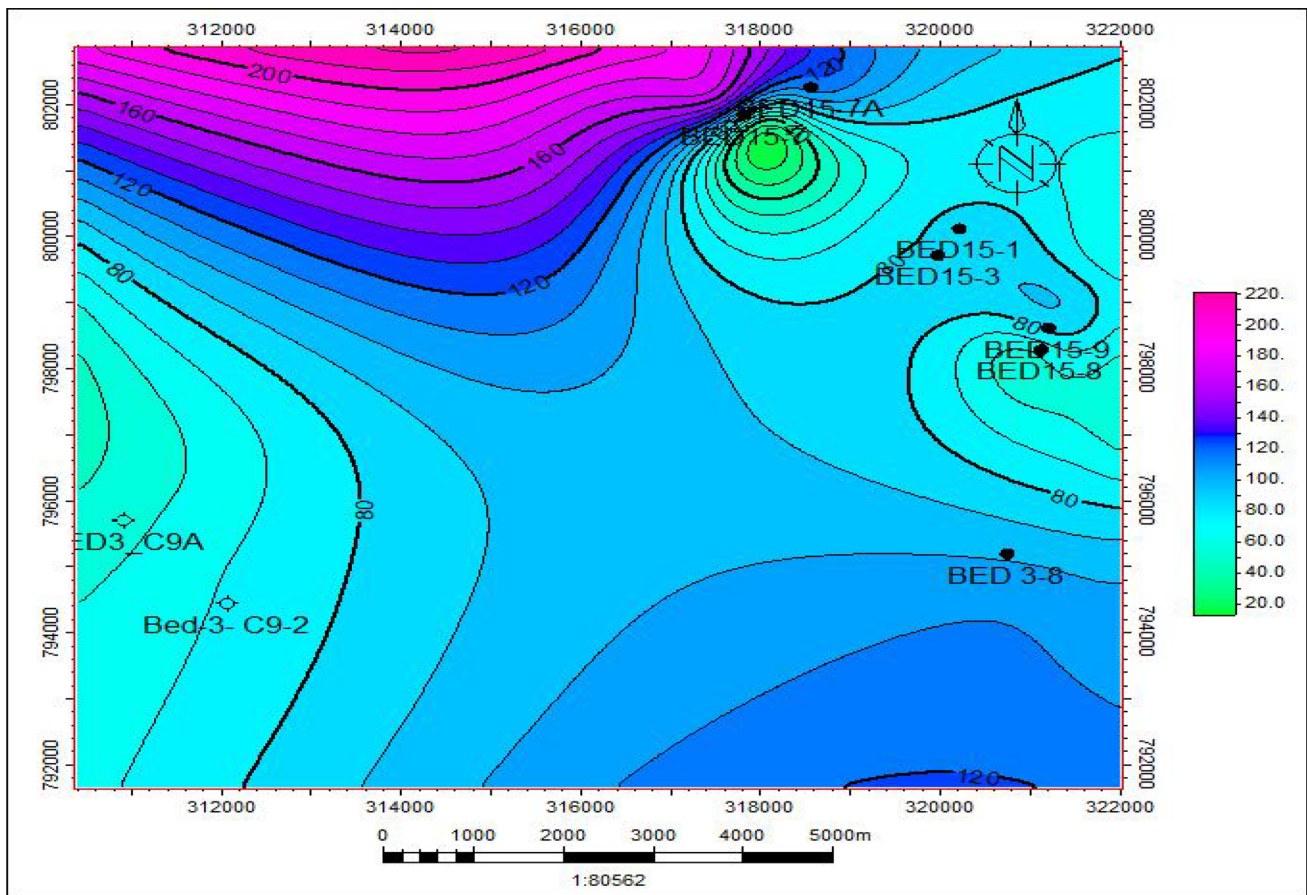


Fig. 8 Isopach map of the Abu-Roash C Member in the study area

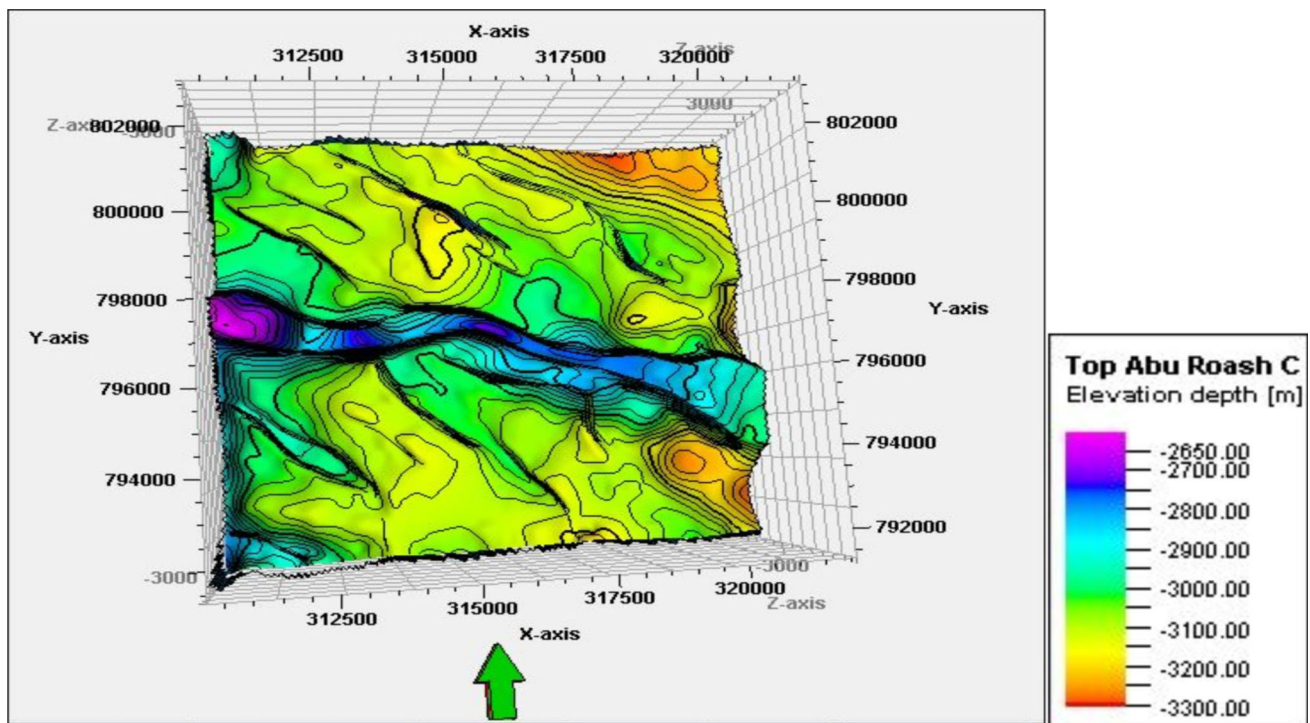


Fig. 9 Top view of the final three-dimensional (3D) structural model of the Upper Abu-Roash C Member

32%, with a maximum of 44% in BED15-9 well. In comparison, the Abu-Roash C Member sandstone shows an average S_w of 12.6% in the BED 3-8 well. The hydrocarbon saturation values are high in most investigated wells of the BED-15 field, averaging 67.7%, with the lowest value of 56.1% in the BED15-9 well and the maximum of 78.8% in the BED 15-3 well. The hydrocarbon saturation value is high only in the BED 3-8 well of the BED-3 field, with the highest value of 87.4% in this study.

4.2.2 Hydrocarbon Potential

Typically, petrophysical properties gathered from the borehole analysis are diverse laterally and vertically, and so two primary steps have been undertaken during the study of oil situation. The first step is studying the lateral distribution or variation of petrophysical properties in the area; an iso-parametric chart of net pay, shale content, effective porosity, and petroleum saturation (Fig. 12) gives a pure vision of petroleum potential in the study area. The determination of vertical spread of the petrophysical properties is the second step, which is completed using the petrophysical data log derived from the software techniques.

4.3 Lateral Variations

The lateral distribution of petrophysical features was examined via iso-parametric charting of specific parameters,

which gives a clear vision of the lateral changes and the factors governing them (Fig. 12). The iso-parametric chart displays the data in Table 2 for pay averages per well of the Abu-Roash C Member in BED-3 and BED-15 fields.

4.3.1 Net Pay Mapping

A net pay map was created to show the lateral distribution changes in the effective thickness (H_{eff} %) of the investigated rock beds. Figure 13A explains the net pay thickness distribution of the Abu-Roash C Member sandstone. This reservoir shows high net pay values, which are related to the high hydrocarbon saturation values where the primary depocenter of the study area is located. However, the net pay values decrease in other parts of the study area and vanish in the BED 3-C9-A and BED3-C9-2 wells. These variations point to the sedimentation slope in the Abu-Roash C Member created from the depocenter to the other areas.

4.3.2 Shale Volume Mapping

The shale volume is an important petrophysical property that represents the quality of the reservoir; low shale content commonly indicates a good reservoir. Figure 13B shows the distribution of shale in the Abu-Roash C Member sandstone. It ranges between 6.5% and 10% in the BED-15 field and reaches the maximum value of 12% in the BED 3-C9-A dry well.

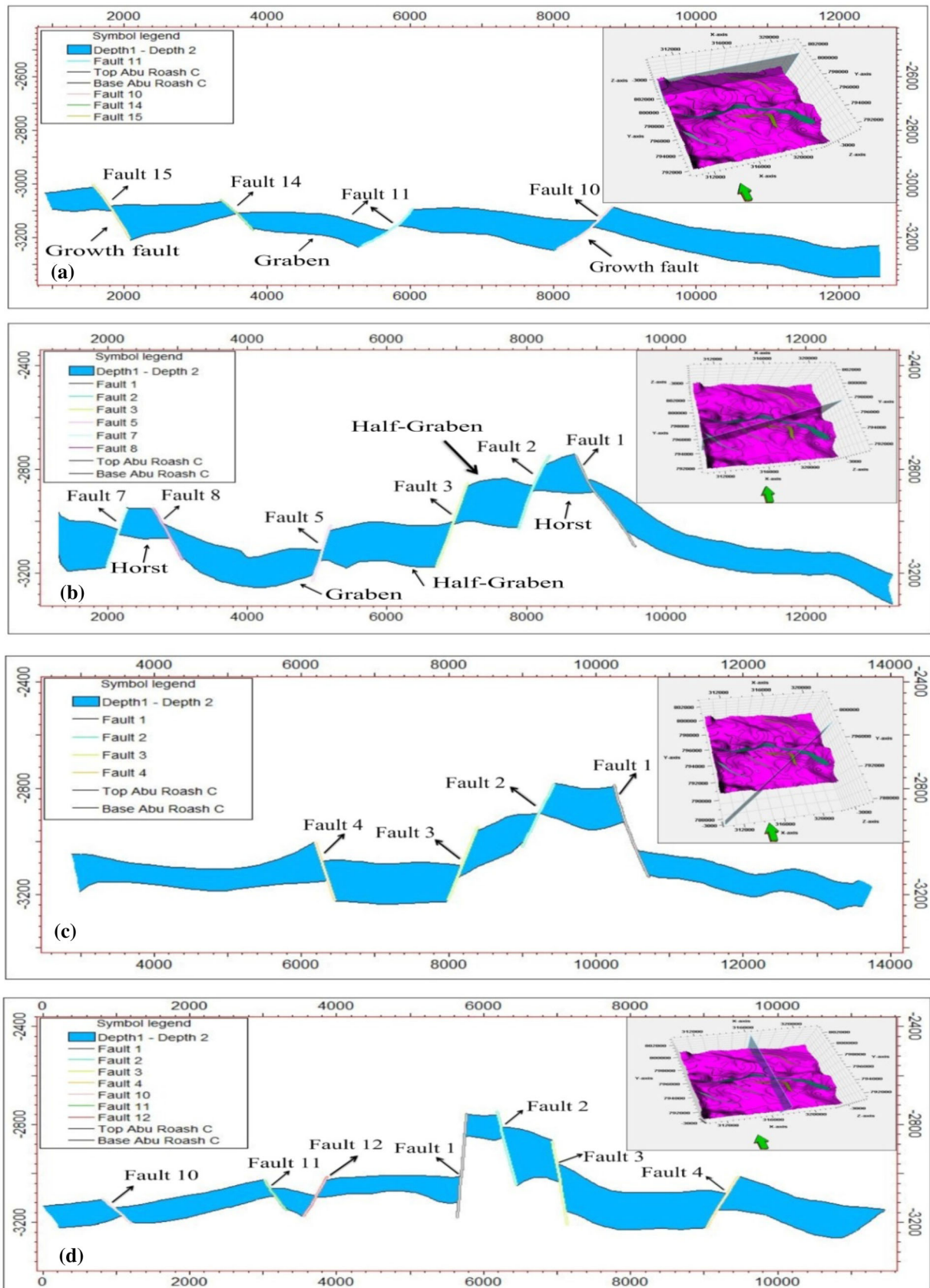


Fig. 10 (a–d) Cross-sections extracted from the three-dimensional (3D) structural model to identify the detailed structural configuration of the Upper Abu-Roash C Member



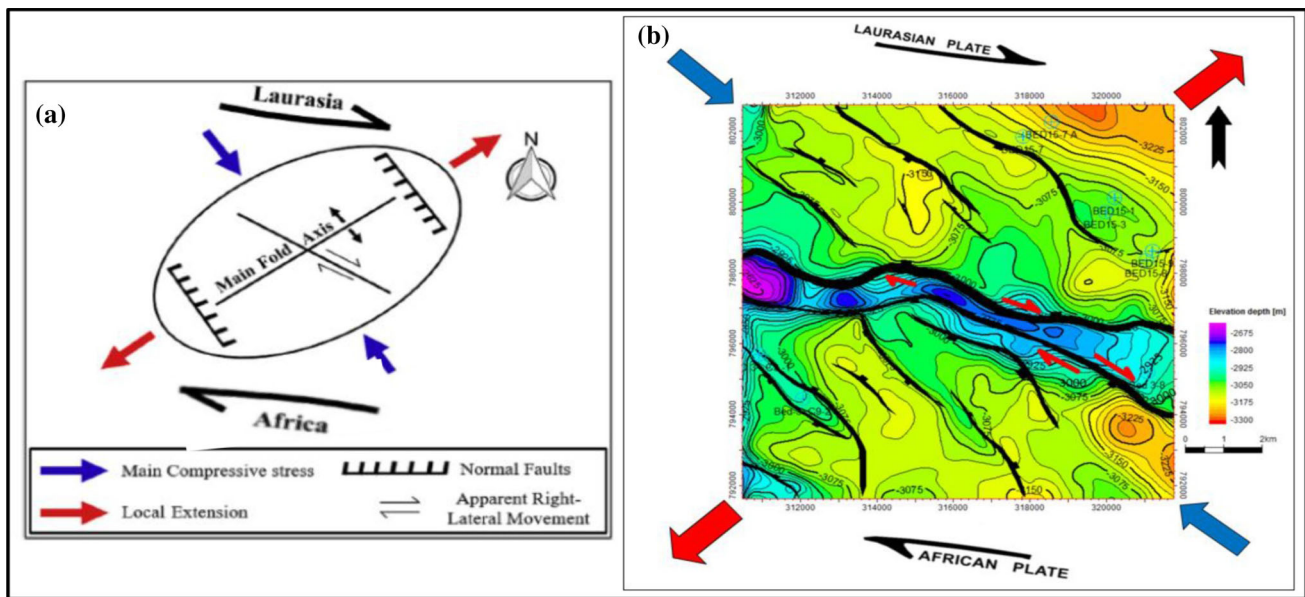


Fig. 11 Dextral wrench model (adopted by the present work). **a** The main interpreted structural trends in the Upper Abu-Roash C Member with respect to the plate tectonic movements. The interpreted NE–SW trending compressional fold and NW–SE trending faults formed as a result of the right-lateral translational movement of Africa relative to Laurasia in the Late Cretaceous [4, 12, 20, 25]. **b** Clearly represents the related structures of the dextral wrench tectonic in the study area within

the Abu Gharadig Basin. the red arrows represent the related extension trend that formed the NW–SE normal faults perpendicular to the maximum stretching axis, and the blue arrows represent the NE–SW compression that produced the mapped NE–SW en echelon anticline perpendicular to the minimum stretching axis, the black half arrows show the dextral wrench tectonics that affected the entire study area, and the red half arrows show an example of the apparent right-lateral movement for the anticline contours along the intersected normal fault

4.3.3 Effective Porosity Mapping

Effective porosity is the most important petrophysical property in assessing petroleum potential. Structural elements have a great effect on porosity improvement[30]. Figure 13C shows the distribution of the effective porosity of the Abu-Roash C Member sandstone. The maximum value of the effective porosity is 32.6% in the BED 15-7 well of the BED-15 field. However, the highest porosity value is 32.6% from the BED-3 field in the BED 3-8 well.

4.3.4 Hydrocarbon Saturation Mapping

Determination of petroleum saturation ($1 - S_w$) is the chief object of the present work. Note that petroleum saturation determination based on the water saturation is a challenging petrophysical computation because different approaches can be used to evaluate S_w . These approaches lead to slightly different S_w values that may result in considerable changes to the original gas in place (OGIP) or the original oil in place (OOIP) volumes. Figure 13D shows the petroleum saturation distribution in the Abu-Roash C Member sandstone. Petroleum saturation ranges between 56.1 and 78.8% in the BED-15 field and equals 87.4% in the BED 3-8 well in the BED-3 field.

4.4 Vertical Variation Setting

Litho-saturation analysis can detect the vertical distribution of lithology (shale content and matrix) and petrophysical properties (porosity as well as the water and hydrocarbon saturation rates) to accurately estimate conditions in the boreholes and compare between multiple boreholes. Figures 14 and 15 show the litho-saturation cross-plots for the BED 15-3 and BED 3-C9-2 wells for the Abu-Roash C Member in BED-15 and BED-3 fields, respectively. As per the available core data and litho-saturation analysis, the Abu-Roash C Member essentially combines siltstone, shale, and sandstone with a few streaks of limestone, which was deposited within a restricted shallow marine shelf.

Figure 14 shows the petrophysical data log of the Abu-Roash C Member in BED 15-3 well. This section shows that the lower part of the Abu-Roash C Member is composed of sandstone with shale intercalations and represents the main net pay interior reservoir in most wells. The V_{cl} track demonstrates that the average shale volume is 10% in the net pay zone, but the shale volume distribution is not uniform. The shale content decreases in the lower section along with all net pay zones and increases in the other parts of the reservoir to as much as 34%. Moreover, the porosity track shows that the average effective porosity for the lower part of the net pay zone equals 16.67% and is 20.15% for the entire net pay

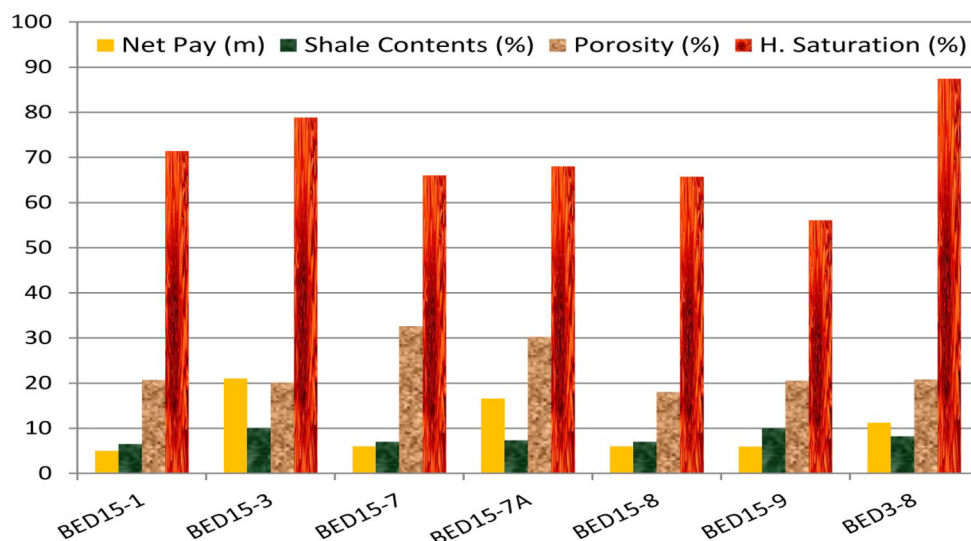


Fig. 12 A chart summarizing the calculated petrophysical parameters (net pay, shale volume, effective porosity, and hydrocarbon saturation) for the promising zones

thickness. In comparison, the average porosity of all reservoirs in the study area is 18.3%. Moreover, the saturation track presented indicates that the S_w decreases through the net pay zone and increases in the other parts of the reservoir. The hydrocarbon occurrence increases in the base section as the shale ratio is low and decreases in the upper section because of the high shale ratio.

Figure 15 shows an example of a nonprospective well with the minimum shale occurrence (average 11%) and maximum porosity (average 16.8%) along with low-resistivity pay (average deep resistivity $0.96 \Omega \text{ m}^{-1}$) in the reservoir zone. A low-resistivity pay is usually recognized by low readings for the deep resistivity curves (generally $\sim 0.5\text{-}\Omega \text{ m}$ to $5\text{-}\Omega \text{ m}$) or by low contrast in the responses of the resistivity log caused by a variety of factors related to mineralogy, microporosity, and water salinity, as well as layer dip, thickness, and anisotropy. The low-contrast pay zone suggests a lack of deep resistivity contrast between pay sands and wet zones or adjacent shale. Therefore, it is difficult to differentiate between pay and wet zones. Possible reasons for low-contrast or low-resistivity pay zones are mentioned in detail in [31]. According to [32] and [33], a low-contrast pay zone estimates laminated sand–shale reservoir areas, particularly at the dry oil productive wells indicated by high clay volumes. The application of this method in this state is important to confirm the excess conductivity increase compared with the surrounding rock. This method depends on the integration between conventional logging results and tested samples or core measurements to confirm and calibrate both clean and shaly-sand electrofacies as well as on the anisotropy, which is the important factor in correcting the apparent vertical resistivity. Finally, we can describe this hole with water-bearing

sand depending on the log evaluation results, but we lack the data to validate this conclusion.

The results of the petrophysical analysis can be summarized based on the results of core data and well logging. The Abu-Roash C Member comprises siltstone, shale, and sandstone intercalated with streaks of limestone. In the BED-3 field, a total of 11 m of net pay sand was calculated to have an average porosity of 20.8% and hydrocarbon saturation of 87.4%, and production was tested at 2337 barrels per day (b/d) of oils of 42.2 OAPI and 2.215 million standard cubic feet per day (MMscf/d) of gas in well BED 3-8. Thus, the BED 3-8 well area has optimum reservoir potential as per the criteria set by [34] and [35] after [36]. The Abu-Roash C Member in the area of wells BED 3-C9-1 and BED 3-C9-2 is not prospective. In BED-15, net pay sand within the Abu-Roash C Member range between 5-m and 21.04-m-thick, and the average porosity ranges from 18 to 32.6%. However, the hydrocarbon saturation ranges between 56.1, and 78.8% and production was tested at 3220 b/d of oil at 36.4 OAPI and 0.663 MMscf/d of gas in the BED 15-3 well. The net-to-gross ratio (NTG) describes the sandstone quality within Abu-Roash C Member as a potential sandy reservoir. The reservoir quality is better with higher NTG values [37, 38].

4.5 Calibration of Wireline Log Estimations

According to the report on core Sample Analysis for well BED15-3 in the BED15 field, the core interval of 18 m (3120–3138 mss (meter subsea)) has a net pay thickness of 17.7 m with good reservoir quality (average porosity $\sim 16.5\%$, average horizontal and vertical permeability $kH = 561.84$ and $kV = 352.35 \text{ mD}$) and water saturation $\sim 13\%$

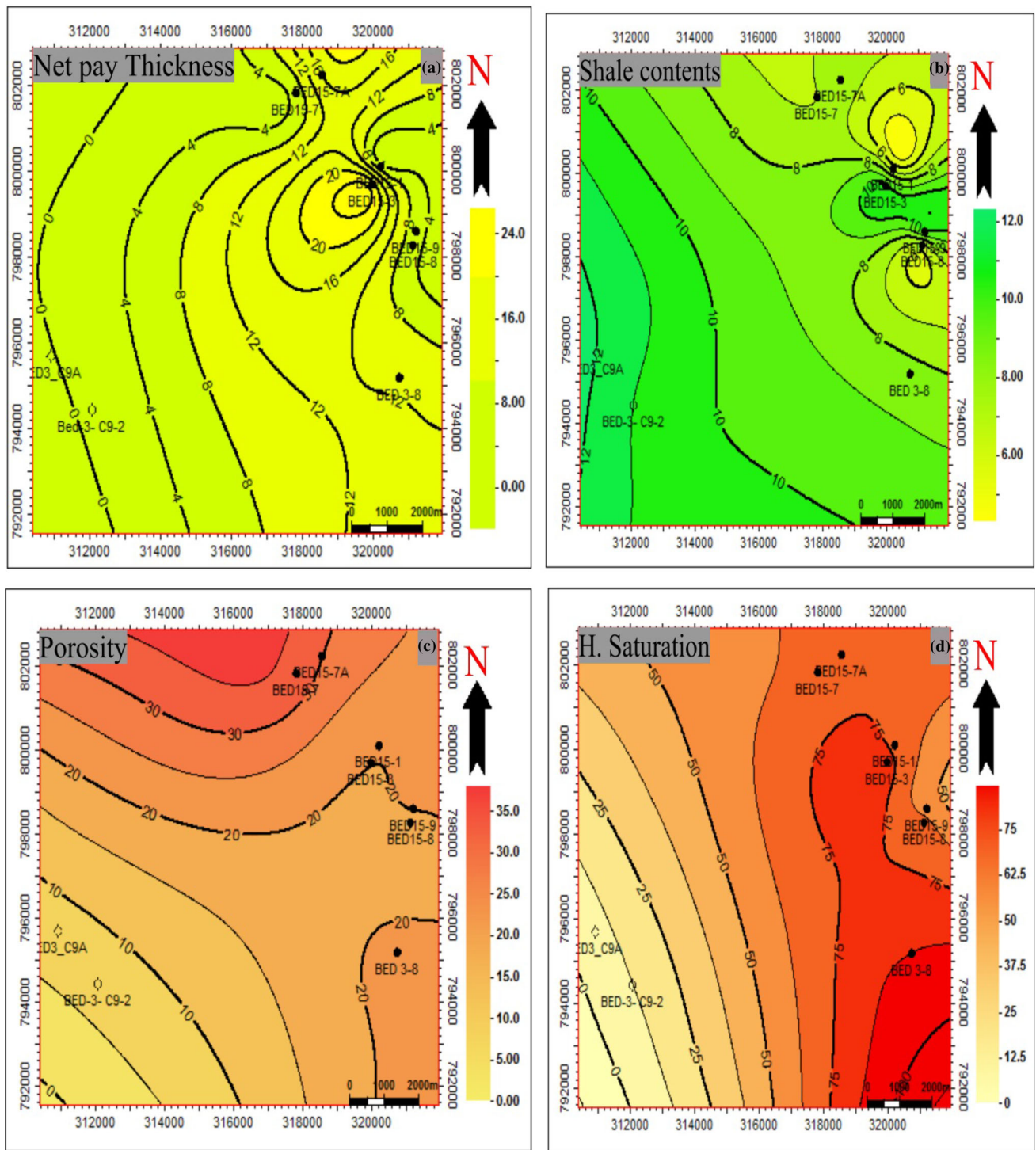


Fig. 13 Iso-parametric maps of Abu-Roash C Member where **a** is the net pay, **b** is the Shale volume, **c** is the effective porosity and **d** is the hydrocarbon saturation

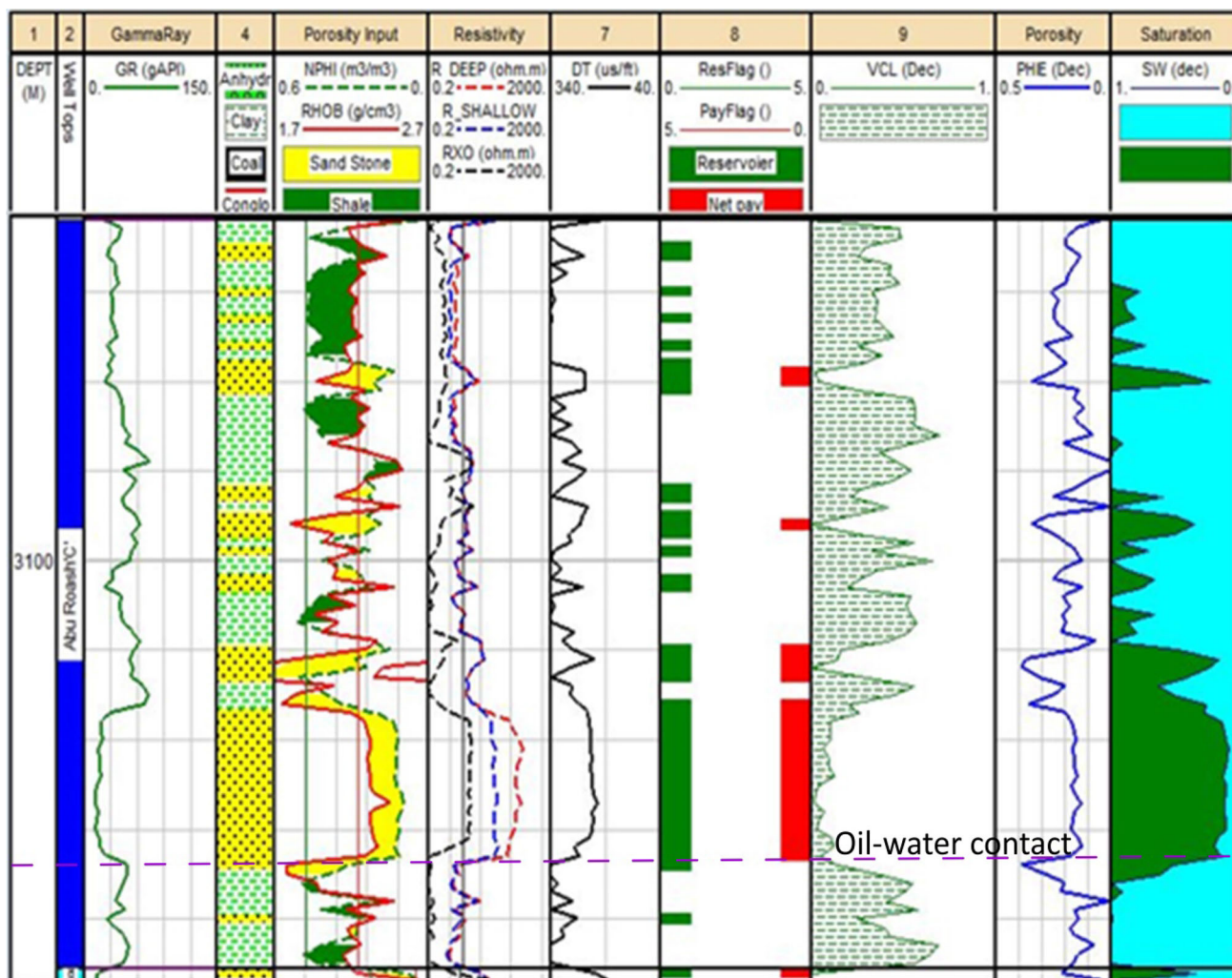


Fig. 14 Litho-saturation cross-plot of the Abu Roash “C” reservoir (BED 15-3 well, as an example of hydrocarbon-bearing sand)

where the oil–water contact is at 3137.7 mss. These results demonstrate that the final measured properties agree with the wireline log estimates in BED15-3, which show that the average effective porosity for the same 18 m-thick net pay zone (3116–3133 mss) equals $\sim 16.67\%$ and water saturation $\sim 14\%$, while the oil–water contact is at 3133 mss (Fig. 14). The core samples description report show that the net pay zone is a clean sandstone. Absolute error in wireline subsea depth for vertical or near-vertical wells is considered to be ± 2 m in the study area.

4.6 Basin Evolution and Petroleum Systems

The BED-3 and BED-15 fields are located in the Abu Gharadig basin, which is a W-E trending intracratonic half-graben system, the structural history of the basin is dominated by two tectonic stages. The Qattara half-graben was influenced by a NE-SW extensional regime until the Cenomanian. WNW-ESE was the dominant normal fault trend. The stress

field shifted to an NW–SE compression regime from the Cenomanian onwards, resulting in dextral wrenching along WNW-ESE trending fault zones. By the Upper Senonian period, this wrenching activity had achieved its pinnacle, as evidenced by NE–SW-oriented compression features. A cyclic alternation of shallow water sandstones, neritic to deepwater limestones, and deepwater shales characterizes the Upper Cretaceous Abu Roash Formation (Fig. 3). The Abu Roash Formation’s transgressive/regressive sedimentary cycles are regionally significant and have been labeled the “A” Member at the top to the “G” Member at the bottom. The carbonates and shale in the “A”, “B”, “D”, and “F” Members were deposited in a neritic environment, whereas the Abu Roash “C”, “E”, and “G” Members comprise coastal plain, lagoonal, and shallow marine sands and shales, as well as some thin limestones. All of these sands have reservoir potential and are oil-bearing in several Abu Gharadig Basin fields. The BED-3 field is also associated with a few smaller antithetic faults, dividing the Abu Roash reservoirs



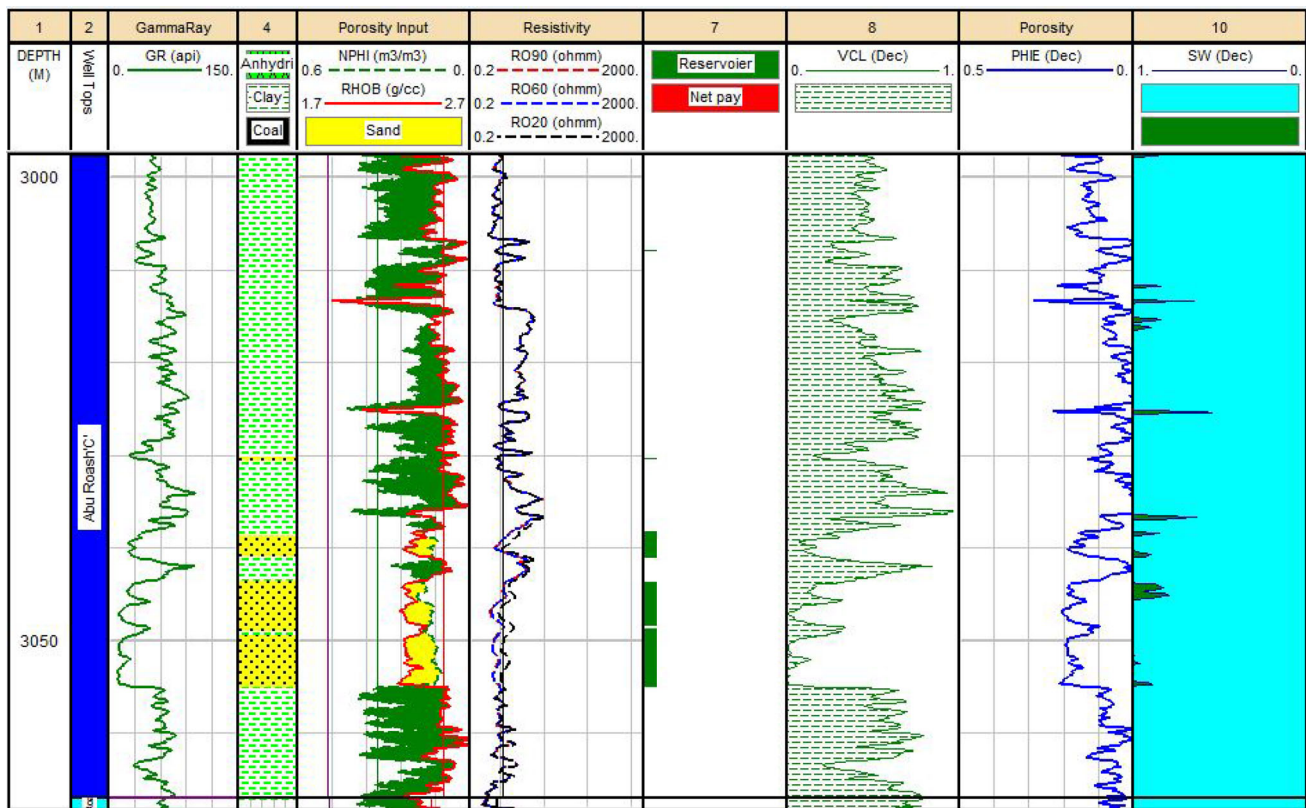


Fig. 15 Litho-saturation cross-plot of the Abu Roash “C” reservoir BED 3-C9-2 well (as an example of a nonprospective well)

into numerous small compartments. Oil pools and pressures in the Abu Roash Formation (Members "C," "E," and "G") have revealed that all faults impacting these reservoirs are sealing, including those with only 20 m of throw [39–41]. In the BED-3 Field’s Abu Roash Formation, no fluid connections have been discovered, and none have been evaluated based on pressure data. In the BED-3 Field, the thin sandstones of the Abu Roash "C" Member contain relatively small amounts of oil. Several of the interbedded shales contain a significant organic content and are believed to be the source of some of the Abu Gharadig Basin’s oil and gas [42]. Also, the hydrocarbon in Bed 15 field is trapped structurally in an NW–SE three-dip closure restricted to the SW by NW–SE south heading normal fault. Minor faults dissect the culmination. They are, however, laterally discontinuous and do not separate the reservoir into blocks at A/R “C” pay level. According to Wali and Ayyad [43], the E, F, and G Members of the Abu Roash Formation have organic-rich horizons and are considered to have fair to good source potential for oil generation. The “F” Member has a high organic content (regionally 1–5%) and is considered to be the main source rock for the Abu Roash oil in the BED-3 and BED-15 Fields [4, 16, 25, 43]. The main Abu Roash reservoir in the current study is a NW–SE tidal-channel sandstone in Abu Roash “C”

with a net pay thickness of up to 11.2 m in BED-3 and a penetrated sand thickness of 5–21 m in the BED-15 field with good reservoir quality. Bayoumi and Mahmoud [44] classified the Abu Roash “C” Member into four units in the BED-3 field, labeled from 1 to 4 in ascending orders. Unit 4 at the top of Abu Roash “C” Member with 30 m thickness is deposited in shallow marine environment; unit 3 with a thickness of 35–40 m is deposited in shallow marine in upper part, and marsh to tidal flat in the lower part; unit 2 is the main reservoir for the Abu Roash "C" Member, with a thickness of 1.5–16 m, and is deposited in a tidal channel in a lagoonal setting, and unit 1 is the lower reservoir, with a thickness of 13–22 m and deposited in a brackish lagoon.

5 Conclusion

This study discusses and estimates the structural setting, petrophysical parameters, and petroleum potential of the Abu-Roash C Member within the BED-3 and BED-15 petroleum fields of the Abu-Gharadig sedimentary basin in the northern part of the Egyptian Western Desert. Nine exploratory wells and 30 2D seismic lines were used for this work. Based on the analysis of the seismic data, the interpreted faults describe the fields’ structural setting, which

includes two major faults together with some synthetic and antithetic faults. These faults have trends ranging between ESE–WNW and NW–SE. As per the cross-sections generated from the 3D seismic model, the faults form grabens, half-grabens, and horsts that are promising for hydrocarbon accumulation. From the petrophysical analysis, the Abu-Roash C Member in BED-15 and the area of BED-3 near BED-15 have the best chance to produce hydrocarbons, where the petrophysical analysis shows that the hydrocarbon saturation of BED 3-8 well is ~ 87.4% and between 56.1 and 78.8% in BED-15. However, the northwest part of the study area near wells BED 3-C9-1 and BED 3-C9-2 is not prospective.

Funding Open access funding provided by The Science, Technology & Innovation Funding Authority (STDF) in cooperation with The Egyptian Knowledge Bank (EKB).

Open Access This article is licensed under a Creative Commons Attribution 4.0 International License, which permits use, sharing, adaptation, distribution and reproduction in any medium or format, as long as you give appropriate credit to the original author(s) and the source, provide a link to the Creative Commons licence, and indicate if changes were made. The images or other third party material in this article are included in the article's Creative Commons licence, unless indicated otherwise in a credit line to the material. If material is not included in the article's Creative Commons licence and your intended use is not permitted by statutory regulation or exceeds the permitted use, you will need to obtain permission directly from the copyright holder. To view a copy of this licence, visit <http://creativecommons.org/licenses/by/4.0/>.

References

- Bayoumi, A.I.; Lotfy, H.I.: Modes of structural evolution of Abu Gharadig Basin, Western Desert of Egypt as deduced from seismic data. *J. Afr. Earth Sci. (Middle East)* **9**(2), 273–287 (1989)
- EGPC (Egyptian General Petroleum Corporation). The Western Desert, oil and gas fields, a comprehensive overview. In: EGPC 11th Petroleum Exploration and Production Conference, p. 431 (1992).
- Meshref, W.M.; Abu El Karamat, M.S.; El Gindi, M.K.: In Exploration concepts for oil in the Gulf of Suez (Vol. 1). In: 9th Exploration and Production Conference, Egyptian General Petroleum Corporation, Cairo, pp. 1–23 (1988)
- Sarhan, M.A.: Seismic–Wireline logs sequence stratigraphic analyses and geologic evolution for the Upper Cretaceous succession of Abu Gharadig basin, Egypt. *J. Afr. Earth Sci.* **129**, 469–480 (2017)
- Wescott, W.A.; Atta, M.; Blanchard, D.C.; Cole, R.M.; George, S.T.; Miller, D.A.; O'Hayer, W.W.; Wilson, A.D.; Dolson, J.C.; Sehim, A.: PS Jurassic Rift Architecture in the Northeastern Western Desert, Egypt (2011)
- Guiraud, R.: Mesozoic rifting and basin inversion along the northern African Tethyan margin: an overview. *Geol. Soc. Lond. Spec. Publ.* **132**(1), 217–229 (1998)
- Bosworth, W.: A model for the three-dimensional evolution of continental Rift Basins, North-East Africa. *Geol. Rundsch.* **83**(4), 671–688 (1994)
- Barakat, M.K.; Nooh, A.Z.: Reservoir quality using the routine core analysis data of Abu Roash “C” in Badr El Din-15 oil field, Abu Gharadig Basin, North Western Desert, Egypt. *J. Afr. Earth Sci.* **129**, 683–691 (2017)
- Khaled, K.A.: Cretaceous source rocks at the Abu Gharadig oil and gasfield, Northern Western Desert, Egypt. *J. Pet. Geol.* **22**(4), 377–395 (1999)
- El Diasty, W.Sh.; Moldowan, J.M.: Application of biological markers in the recognition of the geochemical characteristics of some crude oils from Abu Gharadig Basin, north Western Desert-Egypt. *Marine Petrol. Geol.* **35**(1), 28–40 (2012)
- Sarhan, M.A.; Li, R.E.; Collier, J.: Distinguishing rift-related from inversion-related anticlines: observations from the Abu Gharadig and Gindi Basins, Western Desert, Egypt. *J. Afr. Earth Sci.* **145**, 234–245 (2018)
- Meshref, W.M.: Tectonic framework. In: Said, R., Ed. *The Geology of Egypt*. Rotterdam: Balkema **113**, 155 (1990)
- Guiraud, R.; Bosworth, W.: Phanerozoic geodynamic evolution of northeastern Africa and the northwestern Arabian platform. *Tectonophysics* **315**(1–4), 73–104 (1999)
- Keeley, M.L.: Phanerozoic evolution of the basins of northern Egypt and adjacent areas. *Geol. Rundsch.* **83**(4), 728–742 (1994)
- Stampfli, G.M.: Permo-Mesozoic evolution of the western Tethys realm: the Neotethys East Mediterranean basin connection. *Peri-Tethyan Rift/Wrench Basins and Passive Margins*, pp. 51–108 (2001)
- Lüning, S.; Kolonic, S.; Belhadj, E.M.; Belhadj, Z.; Cota, L.; Barić, G.; Wagner, T.: Integrated depositional model for the Cenomanian-Turonian organic-rich strata in North Africa. *Earth Sci. Rev.* **64**(1–2), 51–117 (2004)
- Garfunkel, Z.: Origin of the Eastern Mediterranean basin: a reevaluation. *Tectonophysics* **391**(1–4), 11–34 (2004)
- Moustafa, A.R.: Mesozoic-Cenozoic basin evolution in the northern Western Desert of Egypt. In: 3rd Symposium on the Sedimentary Basins of Libya, the Geology of East Libya, vol. 3, pp. 29–46 (2008)
- Mahmoud, H.; Lotfy, H.; Bakr, A.: Structural evolution of JG and JD fields, Abu Gharadig basin, Western Desert, Egypt, and its impact on hydrocarbon exploration. *J. Petrol. Explorat. Prod. Technol.* **9**(4), 2555–2571 (2019)
- Smith, A.G.: Alpine deformation and the oceanic areas of the Tethys, Mediterranean, and Atlantic. *Geol. Soc. Am. Bull.* **82**(8), 2039–2070 (1971)
- Guiraud, R.; Bosworth, W.; Thierry, J.; Delplanque, A.: Phanerozoic geological evolution of Northern and Central Africa: an overview. *J. Afr. Earth Sci.* **43**(1–3), 83–143 (2005)
- Bevan, T.G.; Moustafa, A.R.: *Inverted Rift-Basins of Northern Egypt*. Elsevier (2012)
- Sultan, N.; Abdel Halim, M.: Tectonic framework of northern Western Desert, Egypt and its effect on hydrocarbon accumulations. In: Proceedings of the EGPC 9th Exploration and Production Conference, Cairo. Egyptian General Petroleum Corporation Bulletin, vol. 2, pp. 1–19 (1988)
- Bosworth, W.; Stockli, D.F.; Helgeson, D.E.: Integrated outcrop, 3D seismic, and geochronologic interpretation of Red Sea dike-related deformation in the Western Desert, Egypt—the role of the 23 Ma Cairo “mini-plume.” *J. Afr. Earth Sci.* **109**, 107–119 (2015)
- Abdelmaksoud, A.; Ewida, H.F.; El-Habaak, G.H.; Amin, A.T.: 3D structural modeling of the Upper Bahariya Member in Abu Gharadig oil and gas field, North Western Desert, Egypt. *J. Afr. Earth Sci.* **150**, 685–700 (2019)
- Schlumberger: Well Evaluation Conference, Egypt. Schlumberger Technical Editing Services, Chester (1995)
- Labib, M.: Contributions to the geology of Upper Cretaceous with special emphasis on Turonian–Senonian sedimentation patterns and hydrocarbon potentialities in the Abu Gharadig area, north



- Western Desert, Egypt. Unpublished Dissertation thesis, Geology Department, Cairo University, Cairo, p. 189 (1985)
28. Linari, V.: A practical approach to well-seismic data calibration. *Lead. Edge* **23**(8), 774–775 (2004)
 29. Bisaso, I.: Calibration of seismic and well data: towards improved quantitative seismic reservoir characterisation of the Triassic to Middle-Jurassic Gullfaks Reservoir Units of the northern North Sea. Master's thesis, The University of Bergen (2011)
 30. Attia, M.M.; Abudeif, A.M.; Radwan, A.E.: Petrophysical analysis and hydrocarbon potentialities of the untested Middle Miocene Sidri and Baba sandstone of Belayim Formation, Badri field, Gulf of Suez, Egypt. *J. Afr. Earth Sci.* **109**, 120–130 (2015)
 31. Darling, H.L.; Sneider, R.M.; Moore, D.C.: Productive low resistivity well logs of the offshore Gulf of Mexico: causes and analysis. In: *Productive low resistivity well logs of the offshore Gulf of Mexico: New Orleans Geological Society and the Houston Geological Society*, pp. 23–36 (1993)
 32. Darling, T.: *Well Logging and Formation Evaluation*. Elsevier, Amsterdam (2005)
 33. El-Bagoury, M.: Integrated petrophysical study to validate water saturation from well logs in Bahariya Shaley Sand Reservoirs, case study from Abu Gharadig Basin, Egypt. *J. Petrol. Explorat. Prod. Technol.* **10**(8), 3139–3155 (2020)
 34. Amigun, J.O.; Odole, O.A.: Petrophysical properties evaluation for reservoir characterisation of Seyi oil field (Niger-Delta). *Int. J. Innov. Appl. Stud.* **3**(3), 756–773 (2013)
 35. Shah, S.B.A.; Abdullah, W.H.: Structural interpretation and hydrocarbon potential of Balkassar oil field, eastern Potwar, Pakistan, using seismic 2D data and petrophysical analysis. *J. Geol. Soc. India* **90**(3), 323–328 (2017)
 36. Rider, M.H.: "The geological interpretation of well logs" (1986)
 37. Al-Baldawi, B.A.: Petrophysical evaluation study of Khasib formation in amara oil field, South Eastern Iraq. *Arab. J. Geosci.* **8**(4), 2051–2059 (2015)
 38. Adelu, A.O.; Sanuade, O.A.; Oboh, E.G.; Offeh, E.O.; Adewale, T.; Mumuni, O.S.; Oladapo, I.M.; Omolaiye, E.G.: Hydrocarbon field evaluation: case study of 'Tadelu' field shallow offshore Western Niger Delta, Nigeria. *Arab. J. Geosci.* **9**(2), 1–30 (2016)
 39. Bakry, G.; Eid, A.: Fault/seal paradox in the Abu Gharadig Basin. *Proceedings 14th Petroleum Conference EGPC, Cairo, Exploration* **1**, 81–96 (1996)
 40. El Gazzar, A.M., et al.: Structural evolution of the Abu Gharadig field area, Northern Western Desert, Egypt. *J. Afr. Earth Sci.* **124**, 340–354 (2016)
 41. Salem, et al.: Prospect evaluation of BED 3 and Sitra oilfields, Abu Gharadig Basin, North Western Desert, Egypt. *NRIAG J. Astron. Geophys.* **4**, 222–235 (2015)
 42. Bayoumi, T.: The influence of interaction of depositional environment and synsedimentary tectonics on the development of some Late Cretaceous source rocks, Abu Gharadig Basin, Western Desert, Egypt. In: *Proceedings 13th Petroleum Conference, EGPC, Cairo, Exploration vol. 2*, pp. 475–496 (1996)
 43. Wali, M.; Ayyad, A.A.: Petrology and source potential of Abu Roash "F" Limestone, Abu Sennan - Alam El Shawish area, Western Desert, Egypt: *Proceedings 9th Petroleum Exploration and Production Conference. EGPC, Cairo, Exploration* **2**, 164–188 (1988)
 44. Bayoumi, T.; Mahmoud, A.: An integrated geological and geophysical investigation of the depositional environment of Abu Roash "C" Member in the Badr El Din Leases Area, Western Desert, Egypt: *Proceedings 11th Exploration and Production Conference. EGPC, Cairo, Exploration* **2**, 98–110 (1992)

